NASA/TM-2003-212430
ARL-TR-2998

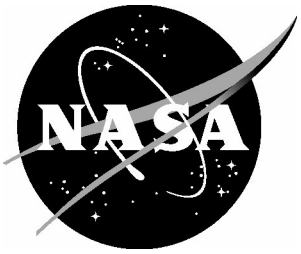

An Approximate Dissipation Function for Large Strain Rubber Thermo-Mechanical Analyses

Arthur R. Johnson and Tzi-Kang Chen
U.S. Army Research Laboratory
Vehicle Technology Directorate
Langley Research Center, Hampton, Virginia

July 2003

The NASA STI Program Office . . . in Profile

Since its founding, NASA has been dedicated to the advancement of aeronautics and space science. The NASA Scientific and Technical Information (STI) Program Office plays a key part in helping NASA maintain this important role.

The NASA STI Program Office is operated by Langley Research Center, the lead center for NASA's scientific and technical information. The NASA STI Program Office provides access to the NASA STI Database, the largest collection of aeronautical and space science STI in the world. The Program Office is also NASA's institutional mechanism for disseminating the results of its research and development activities. These results are published by NASA in the NASA STI Report Series, which includes the following report types:

- TECHNICAL PUBLICATION. Reports of completed research or a major significant phase of research that present the results of NASA programs and include extensive data or theoretical analysis. Includes compilations of significant scientific and technical data and information deemed to be of continuing reference value. NASA counterpart of peer-reviewed formal professional papers, but having less stringent limitations on manuscript length and extent of graphic presentations.

- TECHNICAL MEMORANDUM. Scientific and technical findings that are preliminary or of specialized interest, e.g., quick release reports, working papers, and bibliographies that contain minimal annotation. Does not contain extensive analysis.

- CONTRACTOR REPORT. Scientific and technical findings by NASA-sponsored contractors and grantees.

- CONFERENCE PUBLICATION. Collected papers from scientific and technical conferences, symposia, seminars, or other meetings sponsored or co-sponsored by NASA.

- SPECIAL PUBLICATION. Scientific, technical, or historical information from NASA programs, projects, and missions, often concerned with subjects having substantial public interest.

- TECHNICAL TRANSLATION. English-language translations of foreign scientific and technical material pertinent to NASA's mission.

Specialized services that complement the STI Program Office's diverse offerings include creating custom thesauri, building customized databases, organizing and publishing research results ... even providing videos.

For more information about the NASA STI Program Office, see the following:

- Access the NASA STI Program Home Page at ***http://www.sti.nasa.gov***

- E-mail your question via the Internet to help@sti.nasa.gov

- Fax your question to the NASA STI Help Desk at (301) 621-0134

- Phone the NASA STI Help Desk at (301) 621-0390

- Write to:
  NASA STI Help Desk
  NASA Center for AeroSpace Information
  7121 Standard Drive
  Hanover, MD 21076-1320

NASA/TP-2003-212430
ARL-TR-2998

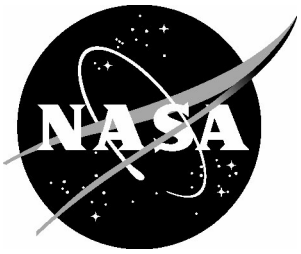

An Approximate Dissipation Function for Large Strain Rubber Thermo-Mechanical Analyses

Arthur R. Johnson and Tzi-Kang Chen
U.S. Army Research Laboratory
Vehicle Technology Directorate
Langley Research Center, Hampton, Virginia

National Aeronautics and
Space Administration

Langley Research Center
Hampton, Virginia 23681-2199

July 2003

Available from:

NASA Center for AeroSpace Information (CASI)
7121 Standard Drive
Hanover, MD 21076-1320
(301) 621-0390

National Technical Information Service (NTIS)
5285 Port Royal Road
Springfield, VA 22161-2171
(703) 605-6000

An Approximate Dissipation Function for Large Strain Rubber Thermo-Mechanical Analyses

Arthur R. Johnson and Tzi-Kang Chen
Army Research Laboratory
NASA Langley Research Center
Hampton, VA 23681-2199

ABSTRACT

Mechanically induced viscoelastic dissipation is difficult to compute. When the constitutive model is defined by history integrals, the formula for dissipation is a double convolution integral. Since double convolution integrals are difficult to approximate, coupled thermo-mechanical analyses of highly viscous rubber-like materials cannot be made with most commercial finite element software. In this study, we present a method to approximate the dissipation for history integral constitutive models that represent Maxwell-like materials without approximating the double convolution integral. The method requires that the total stress can be separated into elastic and viscous components, and that the relaxation form of the constitutive law is defined with a Prony series.

Many commercial codes employ history integral formulations to compute viscous stresses. The numerical approach taken to approximate the history integral often involves an interpolation of the history integral's kernel across a time step. Finite difference equations are then derived for the evolution of the viscous stresses in time. When the material is modeled with a Prony series, the form of these finite difference equations is similar to the form of the finite difference equations for a Maxwell solid. This analogy implies that the value of a Maxwell solid's dissipation function may be close to the value of the dissipation function of a history integral constitutive model. Since the dissipation rate in a Maxwell solid can be easily computed from knowledge of its viscous stress and Prony constants (spring-dashpot constants), we investigated employing the Maxwell solid's dissipation function to couple thermal and large strain mechanical finite element models of rubber. Numerical data is provided to support this analogy and to help understand its limitations. Rubber cylinders with imbedded steel disks and with an imbedded steel ball are dynamically loaded, and the nonuniform heating within the cylinders is computed.

INTRODUCTION

Rubber is employed to carry large loads in tires, gaskets, and tank track pads. It is also used to provide damping and system stability in complex mechanical systems such as helicopter rotors. In these applications, the rubber is typically stiffened by the addition of carbon black. The filled rubber tends to be a poor conductor of heat, yet it also exhibits very large hysteretic energy loss during cyclic loading. Also, the mechanical properties of rubber are strongly dependent on temperature. Faced with the above issues, designers interested in modeling the

detailed response of complex-shaped viscoelastic rubber components need to be able to compute the coupled thermo-mechanical behavior of rubber.

It is computationally difficult to compute dissipation in viscoelastic materials modeled using history integral methods. The dissipation function is expressed as a double convolution integral. Commercial finite element codes that do not compute dissipation for materials with memory lack the ability to perform coupled thermo-mechanical analyses of rubber components.

In this paper, an approximate dissipation function is introduced for viscoelastic materials whose relaxation moduli are modeled with a Prony series. The dissipation function is numerically evaluated for a range of strain rates considered as fast to slow with respect to the Prony series decay rates. The dissipation function is employed to couple the large deformation rubber viscoelasticity and heat transfer finite element algorithms. The resulting thermo-mechanical algorithm is used to simulate the hysteretic heating of dynamically loaded rubber cylinders. Again, the purpose of the work is to establish and test a computational tool for analyzing hysteretic heating in rubber components.

Overviews of large strain rubber viscoelasticity and heat transfer are included to facilitate the description of the thermo-mechanical coupling performed in this study. Only moderate temperature changes were simulated in this study, so time-temperature superposition is not discussed in this effort.

DISSIPATION IN MATERIALS WITH MEMORY

The thermodynamics of materials with memory was formulated and investigated in detail by the early 1970s. We reference a few papers here to provide an overview on the computation of dissipation in materials with memory. Stress wave propagation in viscoelastic solids was investigated in 1961 by Hunter [1]. In his work, Hunter included a discussion of the formulations for thermo-mechanical coupling. A technical presentation of the viscoelastic dissipation in its double convolution integral form was also included. He analytically investigated the coupling effects by studying the case of steady state harmonic strains. Complex modulus methods were then employed to produce a dissipation function.

Several papers by Oden and Aguirre Ramirez [2], Oden and Armstrong [3], and a monograph by Oden [4] present finite element algorithms for thermo-mechanical analyses of materials with memory. In these references, Oden, et al. present the finite element formulation for coupling the equation of motion and the heat conduction equation for materials with memory. To numerically accomplish the coupling, Oden, et al. approximated the viscoelastic dissipation (the double convolution integral) for the case when the material relaxation is represented with a Prony series. They employed finite difference methods for the strain rates and numerical integration for the double convolution integrals.

Using the notation of Hunter [1], the stress in a linear one-dimensional solid can be described as follows

$$\sigma(t) = E\left(\varepsilon(t) - \int_{s=-\infty}^{t} \frac{d\varepsilon(s)}{ds}\phi(t-s)ds\right) \tag{1}$$

where σ is the stress, ε is the strain, t is the current time, and E is the material's elastic modulus. The function ϕ is of the form

$$\phi(t) = \int_{\tau=0}^{\infty} g(\tau)\left(1 - e^{\frac{-t}{\tau}}\right) d\tau \tag{2}$$

in which $g(\tau) > 0$. The viscoelastic rate of energy dissipation, $r(t)$, for this linear solid (see Hunter [1], Oden [4], and Christensen [5]) is expressed with the following double convolution integral

$$r(t) = E \int_{s_2=-\infty}^{t} \int_{s_1=-\infty}^{t} \frac{\partial \varepsilon(s_1)}{\partial s_1} \frac{\partial \varepsilon(s_2)}{\partial s_2} \frac{\partial}{\partial t} \phi(2t - s_1 - s_2) ds_1 ds_2 > 0 \tag{3}$$

Generally, this dissipation function is difficult to evaluate numerically [2, 3, 4].

APPROXIMATION OF DISSIPATION FOR MAXWELL-LIKE MATERIALS

To avoid the computation described in Equation (3) we exploit the fact that when the relaxation modulus in the history integral constitutive model is in a decaying Prony series form (that is, the function ϕ in Equation (2) is described with decaying exponentials) then the history integral can be approximated with a finite difference equation that is similar in form to the finite difference equation for a Maxwell solid. We explore the use of the Maxwell solid's dissipation function (which is easily computed from stresses) for approximating mechanically induced heating in viscoelastic solids defined by history integrals.

Dissipation Function for a Maxwell Solid. In a Maxwell solid (see Figure 1) with a spring-dashpot leg having a spring modulus of E^v, a spring strain of ε^v, a dashpot with viscosity of η, and a total dashpot leg strain of ε, the rate of energy dissipation $r(t)$ is given as follows.

$$r(t) = \frac{dissipated\ \ work}{unit\ \ time} = \frac{\left(\eta \frac{d\left(\varepsilon - \varepsilon^v\right)}{dt}\right) d\left(\varepsilon - \varepsilon^v\right)}{dt} \tag{4}$$

or $$r(t) = \frac{\eta\left(\frac{d\varepsilon}{dt} - \frac{d\varepsilon^v}{dt}\right)^2}{\eta} > 0 \tag{5}$$

with $E^v \varepsilon^v = \eta\left(\frac{d\left(\varepsilon - \varepsilon^v\right)}{dt}\right)$ in the spring-dashpot leg. Equation (5) becomes

$$r(t) = \frac{\left(E^v \varepsilon^v\right)^2}{\eta} = \frac{2\left(\frac{1}{2}E^v\left(\varepsilon^v\right)^2\right)}{\eta / E^v} = \frac{2\,U^v}{\tau} > 0 \tag{6}$$

where $U^v(t)$ is the energy in the spring on the spring-dashpot leg (the viscous leg) and $\tau = \eta / E^v$ is the relaxation time. When the rate of dissipation is measured per unit volume, the term $U^v(t)$ is the corresponding energy density. Then, values of $U^v(t)$ can be approximated by the current values of the viscous stress, $\sigma^v(t)$. If the spring-dashpot leg has a time constant given by τ, the resulting rate of energy dissipation per unit volume is given by

$$r(t) = \frac{\left(\sigma^v\right)^2}{E^v \tau} \geq 0 \tag{7}$$

If we assume the Maxwell model has a rubber spring-dashpot leg, and if we compute stretch ratios from knowledge of the viscous stresses, then we can approximate the linear solid's energy density $U^v(t)$ with a rubber energy density function and use it in Equation (6).

Finite Difference Equations for Viscous Stress Components. A simplified one-dimensional version of the finite difference equations (across a time interval $\Delta t = t_{n+1} - t_n$) for the evolution of the viscous stress, $\sigma^v(t)$, in a history integral model employing Prony series material constants is given by [6]

$$\sigma^v_{n+1} = \left\{\left(1 - \frac{\tau}{\Delta t}\left(1 - e^{\frac{-\Delta t}{\tau}}\right)\right)\hat{\sigma}^0_{n+1} + \left(\frac{\tau}{\Delta t}\left(1 - e^{\frac{-\Delta t}{\tau}}\right)\right)\hat{\sigma}^0_n\right\} g + e^{\frac{-\Delta t}{\tau}}\,\sigma^v_n \tag{8}$$

where $\hat{\sigma}^0_n$ is a stress increment computed at time t_n by using the relative deformation gradient between configurations at times t_{n-1} and t_n, and using the instantaneous modulus, E_0, of the material. The analogous finite difference equation for a Maxwell link (obtained by employing the trapezoidal method) is given by

$$\sigma_{n+1}^{v} = \left\{ \frac{\sigma_{n+1}^{0} - \sigma_{n}^{0}}{\left(1 + \frac{\Delta t}{2\tau}\right)} \right\} g \; + \; e^{\frac{-\Delta t}{\tau}} \; \sigma_{n}^{v} \tag{9}$$

where $\left(\sigma_{n+1}^{0} - \sigma_{n}^{0}\right)$ is a stress increment computed using the total strain (i.e., current configuration's strain) and using the instantaneous modulus of the material.

For a time interval in which the stress increment terms, $\{\bullet\bullet\bullet\}g$, in Equations (8) and (9) are approximately equal, or in which the stress increment terms have small values relative to the stress decay term, $e^{\frac{-\Delta t}{\tau}} \; \sigma_{n}^{v}$, the Maxwell model and the history integral model will have stress histories that are approximately equal. In this case, the dissipation functions for the two models will yield approximately equal values for that time interval.

Procedure for a Large Strain History Integral Viscoelasticity Code. In this section we provide an outline of a variational formulation for rubber elasticity, a history integral version of rubber viscoelasticity [6], and a procedure for approximating the viscoelastic dissipation. Notational definitions that are not included here are given in the Appendix. The coordinates of a material point in the reference configuration are indicated by $\mathbf{X} = \{X_1, X_2, X_3\}$ and in the deformed configuration by $\mathbf{x} = \{x_1, x_2, x_3\}$. The vector function $\mathbf{x} = \mathbf{x}(\mathbf{X}, t)$ defines the mapping of points from the reference configuration into the deformed configuration. The Lagrangian method is employed to describe the deformed solid's energy. The virtual work statement, excluding inertial effects, for a deformed solid of volume V and surface area S is

$$\delta W_I = \int_V \boldsymbol{\sigma} : \delta \mathbf{D}_{\mathbf{v}} \, dV = \int_S \delta \mathbf{v}^T \, \mathbf{t} \, dS + \int_V \delta \mathbf{v}^T \, \mathbf{f} \, \mathrm{dV} \tag{10}$$

where $\delta \mathbf{v}$ is a virtual displacement vector, δW_I is the internal energy due to the virtual displacement, $\mathbf{t}$ is the traction stress prescribed over S, $\mathbf{f}$ is the body force vector acting within the volume V, and V_0 is the volume in the undeformed state. When the solid is rubber, the internal energy in Equation (10) is expressed as follows.

$$\delta W_I = \int_{V_0} \left\{ 2 \left[\left(\frac{\partial U}{\partial \bar{I}_1} + \bar{I}_1 \frac{\partial U}{\partial \bar{I}_2} \right) \overline{\mathbf{B}} - \frac{\partial U}{\partial \bar{I}_2} \overline{\mathbf{B}}^2 \right] : \delta \mathbf{e} + J \frac{\partial U}{\partial J} \; \delta \varepsilon^{vol} \right\} dV_0 \tag{11}$$

where U is the hyperelastic strain energy density function defined in this effort as

$$U = \frac{G}{2} \left(\bar{I}_1 - 3 \right) + \frac{K}{2} \left(J - 1 \right)^2 \tag{12}$$

and where G is the shear modulus, and K is the bulk modulus.

Quasi-static deformations of a viscoelastic rubber solid are often modeled by approximating the material constants with a Prony series. That is, the shear and bulk moduli are expressed in the form

$$G(t) = G_0\left[g_\infty + \sum_{i=1}^{N} g_i\, e^{\frac{-t}{\tau_i}}\right] \quad \text{and} \qquad K(t) = K_0\left[k_\infty + \sum_{i=1}^{N} k_i\, e^{\frac{-t}{\tau_i}}\right] \tag{13}$$

where $G_0 = G(t=0)$ and $K_0 = K(t=0)$ are the instantaneous shear and bulk moduli, and the τ_i's denote relaxation time constants. The deviatoric, $\boldsymbol{\sigma}^D$, and hydrostatic, $\boldsymbol{\sigma}^H$, stresses are determined from history integrals as follows.

$$\boldsymbol{\sigma}^D(t) = \boldsymbol{\sigma}_0^D(t) - SYM\left[\sum_{i=1}^{N} \frac{g_i}{\tau_i} \int_{\xi=0}^{t} \mathbf{F}_t^{-1}(t-\xi)\boldsymbol{\sigma}_0^D(t-\xi)\mathbf{F}_t(t-\xi) e^{\frac{-\xi}{\tau_i}}\, d\xi\right] \tag{14}$$

and

$$\boldsymbol{\sigma}^H(t) = \boldsymbol{\sigma}_0^H(t) - \sum_{i=1}^{N} \frac{k_i}{\tau_i} \int_{\xi=0}^{t} \boldsymbol{\sigma}_0^H(t-\xi) e^{\frac{-\xi}{\tau_i}}\, d\xi \tag{15}$$

where $\mathbf{F}_t(t-\xi)$ is the deformation gradient of the deformed shape at time $t-\xi$ relative to the deformed shape at time t. As mentioned above, approximations are made when Equations (14) and (15) are integrated so that the entire history does not have to be convoluted. The approximations depend on the material constants being of Prony series form. Throughout the remainder of this effort only one term in the Prony series is employed, and the Prony series subscripts are dropped.

The following procedure was employed (at each integration point in each finite element) in this study to compute the approximate viscoelastic rate of dissipation (Equation (6)):

Procedure.

A.) Kinematics. Obtain the deformation gradient, $\mathbf{F} = \dfrac{\partial \mathbf{x}}{\partial \mathbf{X}}$, from the finite element (FE) code. Compute the volume change measure, $J = \det(\mathbf{F})$, compute the deformation gradient with the volume change eliminated, $\overline{\mathbf{F}} = J^{1/3}\mathbf{F}$, compute the deviatoric stretch matrix (the left Cauchy-Green strain tensor), $\overline{\mathbf{B}} = \overline{\mathbf{F}} \cdot \overline{\mathbf{F}}^{\mathbf{T}}$, and find the first strain invariant, $\overline{I}_1 = trace\ \overline{\mathbf{B}}$.

B.) Stresses. Obtain the Cauchy stresses, $\boldsymbol{\sigma}$, from the FE code. Compute the hydrostatic stress, $p = -\dfrac{1}{3}\mathbf{I} : \boldsymbol{\sigma}$, compute the deviatoric stress $\mathbf{S} = \boldsymbol{\sigma} + p\,\mathbf{I}$, compute the elastic deviatoric stress,

$\mathbf{S}^E = \frac{2}{J} DEV\left[\left(\frac{\partial U}{\partial \bar{I}_1} + \bar{I}_1 \frac{\partial U}{\partial \bar{I}_2}\right)\overline{\mathbf{B}} - \frac{\partial U}{\partial \bar{I}_2}\overline{\mathbf{B}}^2\right]$. Note, in this effort, we employed an energy density function U that was not a function of $\bar{I}_2$. Then, since $\bar{I}_1 = trace\,\overline{\mathbf{B}}$, our calculation becomes $\mathbf{S}^E = \frac{1}{J} DEV\left[G_E\overline{\mathbf{B}}\right] = \frac{1}{J}\left[G_E\overline{\mathbf{B}} - \frac{1}{3} trace\left(G_E\overline{\mathbf{B}}\right)\right] = \frac{1}{J} G_E\left(\overline{\mathbf{B}} - \frac{\bar{I}_1}{3}\right)$ for the normal stresses and $\mathbf{S}^E = \frac{2}{J} G_E\overline{\mathbf{B}}$ for the shear stresses where $G_E = G_0(1-g)$. The deviatoric viscoelastic stress is computed next using $\mathbf{S}^v = \mathbf{S} - \mathbf{S}^E$. Compute the principal viscoelastic stresses, $\left(S^v_{p1}, S^v_{p2}, S^v_{p3}\right)$, based on $\mathbf{S}^v$. In the case when a rubber energy density function will be used, compute the principal stretches for the viscoelastic part using the following equations [7]:

$$S^v_{p1} - S^v_{p2} = G_v\left(\lambda^2_{1v} - \lambda^2_{2v}\right)$$
$$S^v_{p2} - S^v_{p3} = G_v\left(\lambda^2_{2v} - \lambda^2_{3v}\right)$$
$$S^v_{p3} - S^v_{p1} = G_v\left(\lambda^2_{3v} - \lambda^2_{1v}\right)$$

and the constraint equation $\lambda^2_{1v} \cdot \lambda^2_{2v} \cdot \lambda^2_{3v} = 1$. To solve for the stretches, we converted these equations into a cubic equation of the form

$$x^3 + r \cdot x^2 + s \cdot x + t = 0$$

where $x = \lambda^2_{2v}$, $r = \left(\lambda^2_{1v} - \lambda^2_{3v}\right) = \left(S^v_{p1} - S^v_{p3}\right)/G_v$, $s = -\left(\lambda^2_{1v} - \lambda^2_{2v}\right)\left(\lambda^2_{2v} - \lambda^2_{3v}\right) = -\left(S^v_{p1} - S^v_{p2}\right)\left(S^v_{p2} - S^v_{p3}\right)/G_v^2$, and $t = -1.0$. Following procedures for solving cubic equations, the equation can be reduced to

$$y^3 + p \cdot y + q = 0$$

where $y = x + r/3$, $p = s - r^2/3$ and $q = \frac{2}{27} \cdot r^3 - \frac{r \cdot s}{3} + t$. By solving the above cubic equation and substituting y into the previous equation, the principal stretches $(\lambda_{1v}, \lambda_{2v}, \lambda_{3v})$ can be obtained.

<u>C.) *Dissipation*</u>. In the case when the Maxwell solid is assumed to have a rubber spring-dashpot leg, compute $I_{1v} = \lambda^2_{1v} + \lambda^2_{2v} + \lambda^2_{3v}$. Then compute the viscoelastic energy density with $U^v = \frac{G_v}{2}(I_{1v} - 3)$. The rate of energy dissipation is then approximated with $r(t) = \frac{2U^v(t)}{\tau}$. In

the case when the Maxwell solid is assumed to have a linear spring-dashpot leg, use the viscous deviatoric stresses to compute the rate of dissipation as $r(t) = \dfrac{\mathbf{S}^v : \mathbf{S}^v}{4\, G_v\, \tau}$.

Accuracy of the Dissipation Function for Rubber. The approximations to $r(t)$ described above are evaluated by solving benchmark problems. We select several uniform axisymmetric, plane stress, and plane strain problems (see Figure 2) and determine the dissipation by calculating the work done during closed load-displacement cycles. Three measures of the dissipation are calculated. The cyclic work done by the finite element code's external forces, and the total dissipated work found by integrating Equations (6) & (7) over the solid's volume and over time. The time frames and strain rates in these benchmark examples are selected relative to the Prony series relaxation time τ as follows:

<u>*Case 1*</u>. A generic description of the first cyclic loop employed is given in Figure 3. The loop represents a rapid step-strain loading $(0, t_1)$, followed by a relaxation (t_1, t_2), and then followed by a reduction in strain and load until the loop was effectively closed (t_2, t_3).

<u>*Case 2*</u>. A generic description of the second cyclic loop employed is given in Figure 4. The loop represents a rapid step-strain loading $(0, t_1)$, followed by a relaxation (t_1, t_2), followed by a rapid step-strain unloading to zero load (t_2, t_3), and ending by relaxing until the loop was effectively closed (t_3, t_4).

<u>*Case 3*</u>. Dynamic tension-tension and compression-compression enforced sinusoidal displacements were applied at three frequencies. The frequencies were $\omega = 0.1\text{Hz}$, 1.0Hz, and 10.0Hz (slow to fast relative to the material's viscous relaxation time $\tau = 1.0\,\text{sec}$), see Figures 5 to 7.

The ABAQUS [6] finite element code was employed to determine the work done in closed cycles for each *Case* listed above. The four node rectangular CAX4HT axisymmetric, CPE4HT plane strain, and CPS4T plane stress elements were used. The elastic and viscous material constants used in this accuracy study are $G_0 = 1.0\ MPa$, $g = 0.5$, $\tau = 1.0$, and $K_0 = K_\infty = 3000.\ MPa$. The thermal material constants are listed in Table 1. The finite element code's reaction forces were used to compute the total internal dissipation for each of the cycles. The results are referred to here as $\int F_T\, du$. The *Procedure* listed above for approximating the dissipation was employed to compute the total dissipation in a cycle. The approximate dissipation results are referred to here as $\int r(t)\, dt$. The *Error* is defined as

$$Error = \left[\frac{\int F_T\, du - \int r(t)\, dt}{\int F_T\, du} \right] \tag{16}$$

The error calculations for axisymmetric loading produce data nearly identical with the error data obtained for plane stress. The errors obtained in plane strain are larger than those obtained in plane stress when they are compared relative to the maximum principal strain.

In the case of axisymmetric loading, the accuracy results are listed in Tables 2, 3, and 4. The approximation to the dissipation has an error less than 2.0% for small strain deformations and the error grows large as the strain amplitudes are increased. At maximum tensile strain of 0.10 in Cases 1 and 2, the errors in the approximation to the dissipation are approaching 10%.

At large strains, the errors are large, and corrections are needed if this approach is used. It appears possible to calibrate the error at large strain. For example, Figures 8 and 9 show the error as a function of the maximum principle strain and as a function of the first strain invariant for both plane stress and plane strain. A look-up-table could be constructed based on strain invariants or stretch ratios to provide correction factors at large strains.

In these examples, approximating the dissipation with the formulas for energy in a rubber spring-dashpot Maxwell leg yielded smaller errors than when the energy formula for a linear solid-dashpot Maxwell leg was used. In the nonuniform thermo-mechanical heating examples presented below we did not adjust the approximation to the dissipation with a look-up-table.

THERMO-MECHANICAL HEATING OF RUBBER SOLIDS

Heat Transfer. The variational statement of the energy balance equation for heat transfer, together with Fourier's law, for a deformed solid of volume V, and surface area S is given by

$$\int_V \rho \frac{\mathrm{d}U_\theta}{\mathrm{d}t} \delta\theta \, dV + \int_V \frac{\partial \delta\theta}{\partial \mathbf{x}} \, \mathbf{k} \, \frac{\partial \theta}{\partial \mathbf{x}} \, dV = \int_V \delta\theta \, r \, dV + \int_S \delta\theta \, q \, dS \tag{17}$$

where θ is the temperature, U_θ is the internal thermal energy, ρ is the density, q is the heat flux per unit area, r is the heat supplied per unit volume (the dissipation described above), $\mathbf{k}$ is a conductivity matrix, and $\delta\theta$ is a virtual temperature field satisfying the essential boundary conditions. Equation (17) is used to build the transient heat transfer finite element equations for the rubber solid. The term $\int_V \delta\theta \, r \, dV$ couples Equation (17) to Equation (10).

Finite element discretization of the mechanical and thermal variational statements, Equations (10) and (17), results in systems of time dependent differential equations which approximate the mechanical and thermal response of the solid. Below, we computationally investigate heat buildup in rubber solids by employing the approximate calculation of viscoelastic energy dissipation described in the *Procedure* above.

Finite Element Employed. We present the results for the heating of several 2D uniform and non-uniform axisymmetric models. The eight-node hybrid axisymmetric CAX8RHT element was used, see Figure 10. The interpolation in the element is biquadratic for the displacement, and bilinear for the temperature and pressure. Reduced integration is also employed. The nodal variables employed in the thermal element are the temperatures, θ, at the four corner nodes. The stress element has radial, u_r, and axial, u_z, displacements at the eight nodes and hydrostatic

pressure, p_i, variables at each of the four integration points. The computed heating rates, $r(t)$, are applied in the heat transfer algorithm at the four integration points.

Five cylinders were analyzed for hysteretic heating. Only moderate temperature changes were being simulated so the elastic material constants were not treated as temperature dependent and time-temperature superposition was not employed.

Cylinder Dimensions. There were five different cylinder models. The first four models consisted of two groups of two cylinders each. One group consisted of uniform cylinders and the other group had steel disks at their centers, see Figure 11. The first four cylinders each had a radius of $R = 0.0282\,m$. There were two cylinder heights in each group. The heights were $H = 0.05\,m$, and $0.0125\,m$ respectively. The cylinders were compressed between steel fixtures. The model simulates the case when a lubricant maintains the fixture-rubber interface as frictionless. The internal steel disks were completely attached (bonded) to the rubber. The height and radius of the disks were $0.0025\,m$, and $0.0141\,m$ respectively. The fifth model was a tall cylinder of height $0.10m$. This tall cylinder had a steel ball imbedded at its center. The radius of the rubber cylinder was $0.05m$ and the radius of the steel ball was R=$0.025m$. The boundary conditions were the same as those used for the imbedded disk models.

Rubber and Steel Properties. The elastic constants used for the steel are; Young's modulus $E = 206.8\ G\,Pa$, and Poisson's Ratio $\nu = 0.3$. The rubber energy density was modeled as a Neo-Hookean [7] solid, Equation (12). The viscous behavior was described with one Prony series term, Equation (13). The material constants employed are representative of filled rubber [8, 9]. They are; $\frac{G_0}{2} = 1.155\,MPa$, $\frac{k_0}{2} = \frac{k_\infty}{2} = 1.000 * 10^3\,MPa$, and $g = 0.3,\ k = 0.0,\ \tau = 0.1\,\mathrm{s}$. The thermal material constants for both the steel and the rubber are listed in Table 1. The film heat transfer coefficients for the rubber-air and rubber-steel interfaces are $h_A = 5.44284 J/\left(^\circ C\,m^2\,\mathrm{s}\right)$ and $h_S = 20934\ J/\left(^\circ C\,m^2\,\mathrm{s}\right)$, respectively.

Enforced Displacement. The deformation of the tall ($H = 0.05\,m$) uniform cylinder subjected to an axial displacement is shown in Figure 12. Since the boundary conditions are symmetric, only the half height (r, z)-quadrant is shown. The mesh refinement near the top and outer edges is to accommodate the heat transfer gradients at those locations. Each cylinder was subjected to an axial enforced displacement that produced moderately large strain hysteresis. The half height enforced axial displacement for the tall cylinder is described as follows. The top end of the cylinder was ramped to a displacement of $-0.0045\,m$ in $0.05\,s$. The top end of the cylinder was then forced to follow the prescribed axial displacement given by

$$u_z(t) = -0.0045 - 0.0030\,Sin(2\pi(6.5)t) \quad m \tag{15}$$

The half height enforced axial displacement for the short cylinder is described as follows. The top end of the cylinder was ramped to a displacement of $-0.001125\,m$ in $0.05\,s$. The top end of the cylinder was then forced to follow the prescribed axial displacement given by

$$u_z(t) = -0.001125 - 0.00075\,Sin(2\pi(6.5)t) \quad m \tag{16}$$

where t is the time in seconds. The loading and the displacement of the top of the cylinder are shown in Figure 13 for a time interval of 1.0 s. As expected, the displacement curve demonstrates viscoelastic softening. A number of analyses were performed to test the nonlinear elastic, the viscoelastic, and the transient heat transfer finite element algorithms separately. Hand calculations and finite difference calculations verified that the algorithms functioned correctly. The thermal boundary conditions did not significantly affect the temperature fields computed. The following analyses were performed, employing the dissipation function described previously, to investigate the uniform and non-uniform heating of rubber cylinders undergoing large strain dynamic deformations.

Uniform Cylinders. The cyclic deformations given by Equations (15) and (16) were applied to the tall and short uniform cylinders indicated by the dimensions given previously. The temperatures, at the center of the cylinders $(r = 0, z = 0)$ as a function of time for the first 20 s of loading are shown in Figure 14. The frictionless rubber-fixture boundary condition allows the strains to be uniform in the cylinder. Rubber is a poor conductor of heat, and the fact that the cylinders heated nearly uniformly regardless of height was expected.

Cylinders with Imbedded Disks. The models for the tall and short uniform cylinders described above were modified by imbedding steel disks at their centers. The models were cyclically loaded to simulate nonuniform viscoelastic heating in rubber solids when the deformations produce moderately large strains. The results obtained appear reasonable. Figure 15 shows the meshes on the reference and deformed shapes for the tall cylinder. The temperature distribution in the tall block after 20 s of dynamic loading is shown in Figure 16. Temperatures at points A, B, C, and D in Figure 16 are plotted as a function of time in Figure 17. The outer radial end of the internal disk (point C) is predicted to heat much faster than the rest of the cylinder.

Similar results were obtained for the short cylinders. However, there were some convergence problems that were overcome by re-meshing near the top outer corner of the steel insert and employing lower order displacement interpolations (a four node displacement element was employed.) The temperature distribution in the short cylinder is shown in Figure 18. Again, Figure 19 shows that the region of moderately large strains, located near the outer radial end of the internal disk (point C), has the most rapid rise in temperature.

Cylinder with Imbedded Ball. A tall rubber cylinder (H=0.10m) was modeled with an internal steel ball, see Figure 20. The properties and boundary conditions are the same as those employed for the models with the imbedded steel disks described previously. Note, this cylinder is much longer than the cylinders analyzed above and the overall deformation of this cylinder is less severe than the cases analyzed above. The top end of the cylinder was forced to follow a prescribed axial displacement given by Equation (15). The reference and deformed meshes are shown in Figure 21. The strains are moderately large. A temperature distribution profile after 20 s is shown in Figure 22. The region above the ball near the surface of the cylinder is predicted to heat the fastest. The temperatures at these locations as a function of time are shown in Figure 23.

CONCLUDING REMARKS

In dynamically loaded rubber structures predictions of both the strain and the temperature distributions are required to perform degradation studies. A procedure that couples a viscoelastic large deformation stress analysis with a heat transfer analysis to model nonuniform hysteretic heating in rubber was described. The ABAQUS finite element code was used to implement the procedure.

Computations were made to demonstrate the thermo-mechanical heating of tall and short uniform rubber cylinders. The viscoelastic material properties employed are valid for moderately large strain deformations of rubber. When the time dependent strains in the cylinders were uniform, the heating computed was also uniform. The thermo-mechanical heating of tall and short rubber cylinders, containing internal steel disks and a steel ball were also computed. The internal steel components provided high strain gradients within the rubber cylinders and nonuniform hysteretic heating was observed. The analyses performed suggest that the coupling procedure should be considered for further development as a design tool for rubber degradation studies.

REFERENCES

1. Hunter, S. C., "Tentative equations for the propagation of stress, strain, and temperature fields in viscoelastic solids," J. Mech. Phys. Solids, Vol. 9, pp. 39-51, 1961.
2. Oden, J. T., and Aguirre Ramirez, G., "Formulation of general discrete models of thermomechanical behavior of materials with memory," Int. J. Solids Structures, Vol. 5, pp. 1077-1093, 1969.
3. Oden, J. T., and Armstrong, W. H., "Analysis of nonlinear, dynamic coupled thermoviscoelasticity problems by the finite element method," Computers and Structures, Vol. 1, pp. 603-621, 1971.
4. Oden, J. T., *Finite Elements of Nonlinear Continua*, McGraw-Hill Book Company, Library of Congress number 70-154237, 1972.
5. Christensen, R. M., *Theory of Viscoelasticity, An Introduction*, Academic Press, Library of Congress Number 74-127681, 1971.
6. Hibbitt, Karlsson & Sorensen Inc., *ABAQUS Theory Manual, Version 5.8*, 1080 Main St., Pawtucket, RI., 2000.
7. Treloar, L. R. G., *The Physics of Rubber Elasticity*, Clarendon Press, ISBN 0 19 851355 0, 1975.
8. Clark, S. K. and Dodge, R. N., "Heat Generation in Aircraft Tires Under Braked Rolling Conditions," NASA Contractor Report 3629, 1982.
9. Pitts, D. R. and L. E. Sissom, L. E., *Heat Transfer*, McGraw-Hill Book Co., Library of Congress number 77-20255, 1977.

APPENDIX

The following notation is included to assist the reader with the description of the finite element algorithm for rubber viscoelasticity.

$X_i\ (i = 1,2,3)$	coordinates of a material point in the reference configuration.
$x_i\ (i = 1,2,3)$	coordinates of a material point in the deformed configuration.
$\mathbf{x} = \mathbf{x}(\mathbf{X}, \mathrm{t})$	vector mapping between the reference and deformed configurations.
$\mathbf{F} = \dfrac{\partial \mathbf{x}}{\partial \mathbf{X}}$	deformation gradient.
$J = \det(\mathbf{F})$	determinate of $\mathbf{F}$ which measures volume change.
$\overline{\mathbf{F}} = J^{-\frac{1}{3}}\mathbf{F}$	deformation gradient scaled for volume change.
$\overline{\mathbf{B}} = \overline{\mathbf{F}}\,\overline{\mathbf{F}}^T$	left Cauchy Green strain tensor.
$\bar{I}_1 = tr(\overline{\mathbf{B}})$	first strain invariant (adjusted for volume).
$\bar{I}_2 = \dfrac{1}{2}\left(\left(\bar{I}_1^2\right) - tr(\overline{\mathbf{B}}\,\overline{\mathbf{B}})\right)$	second strain invariant (adjusted for volume).
$\delta\mathbf{u}$	displacement.
$\delta\mathbf{L} = \dfrac{\partial \delta\mathbf{u}}{\partial \mathbf{x}}$	gradient of displacement.
$\delta\mathbf{D} = \dfrac{1}{2}\left(\delta\mathbf{L} + \delta\mathbf{L}^T\right)$	rate of deformation.
$\delta\mathbf{D}_\mathbf{v}$	rate of deformation computed using virtual displacement $\delta\mathbf{v}$.
$\mathbf{A} : \mathbf{B}$	scalar product of matrices $\mathbf{A}$ and $\mathbf{B}$.
$\delta\varepsilon^{vol} = \mathbf{I} : \delta\mathbf{D}$	volumetric strain rate.
$\delta\mathbf{e} = \delta\mathbf{D} - \dfrac{1}{3}\delta\varepsilon^{vol}\mathbf{I}$	deviatoric strain rate.
$p = -\dfrac{1}{3}\mathbf{I} : \boldsymbol{\sigma}$	pressure stress (hydrostatic).

TABLES

Table 1. Thermal properties.

Property	Rubber	Steel
Conductivity, $J/(^{\circ}C\,m\,\mathrm{s})$ $\kappa =$	0.20934	45.83379
Density, kg/m^3 $\rho =$	1000.	7849.
Specific heat, $J/(kg\,^{\circ}C)$ $c =$	2093.4	460.
Expansion, $(^{\circ}C)^{-1}$ $a =$	$80.*10^{-6}$	$12.*10^{-6}$

Table 2. Errors obtained predicting dissipation, Case 1, see Figure 3.

		$r(t)=\frac{2U^v(t)}{\tau}$ $U^v=\frac{G_v}{2}(I_1^v-3)$	$r(t)=\frac{\mathbf{S}^v:\mathbf{S}^v}{4\,G_v\,\tau}$
Loading	Maximum strain	*Error*	*Error*
Tension	0.01	0.0045	0.0087
Tension	0.10	0.0273	0.0719
Tension	0.50	0.1428	0.4260
Tension	1.00	0.2923	1.021
Compression	-0.01	-0.0003	-0.0045
Compression	-0.10	-0.0200	-0.0591
Compression	-0.50	-0.0334	-0.1800

Table 3. Errors obtained predicting dissipation, Case 2, see Figure 4.

		$r(t)=\dfrac{2U^v(t)}{\tau}$ $U^v=\dfrac{G_v}{2}\left(I_1^v-3\right)$	$r(t)=\dfrac{\mathbf{S}^v:\mathbf{S}^v}{4\,G_v\,\tau}$
Loading	Maximum strain	*Error*	*Error*
Tension	0.01	0.0064	0.0088
Tension	0.10	0.0420	0.0654
Tension	0.50	0.2450	0.3890
Tension	1.00	0.5610	0.9330
Compression	-0.01	-0.0036	-0.0054
Compression	-0.10	-0.0359	-0.0567
Compression	-0.50	-0.1110	-0.1810

Table 4. Errors obtained predicting dissipation, Case 3, see Figure 5.

				$r(t)=\dfrac{2U^v(t)}{\tau}$ $U^v=\dfrac{G_v}{2}\left(I_1^v-3\right)$	$r(t)=\dfrac{\mathbf{S}^v:\mathbf{S}^v}{4\,G_v\,\tau}$
Loading	Frequency Hz	Minimum strain	Maximum strain	*Error*	*Error*
Tension	0.10	0.004	0.02	0.0131	0.0131
Tension	0.10	0.10	0.50	0.3830	0.3820
Tension	1.0	0.004	0.02	0.0132	0.0132
Tension	1.0	0.10	0.50	0.3760	0.3820
Tension	10.0	0.004	0.02	0.0136	0.0137
Tension	10.0	0.10	0.50	0.3720	0.3840
Compression	0.10	-0.004	-0.02	-0.0109	-0.0109
Compression	0.10	-0.10	-0.50	-0.1810	-0.1830
Compression	1.0	-0.004	-0.02	-0.0108	-0.0108
Compression	1.0	-0.10	-0.50	-0.1730	-0.1830
Compression	10.0	-0.004	-0.02	-0.0102	-0.0104
Compression	10.0	-0.10	-0.50	-0.1700	-0.1840

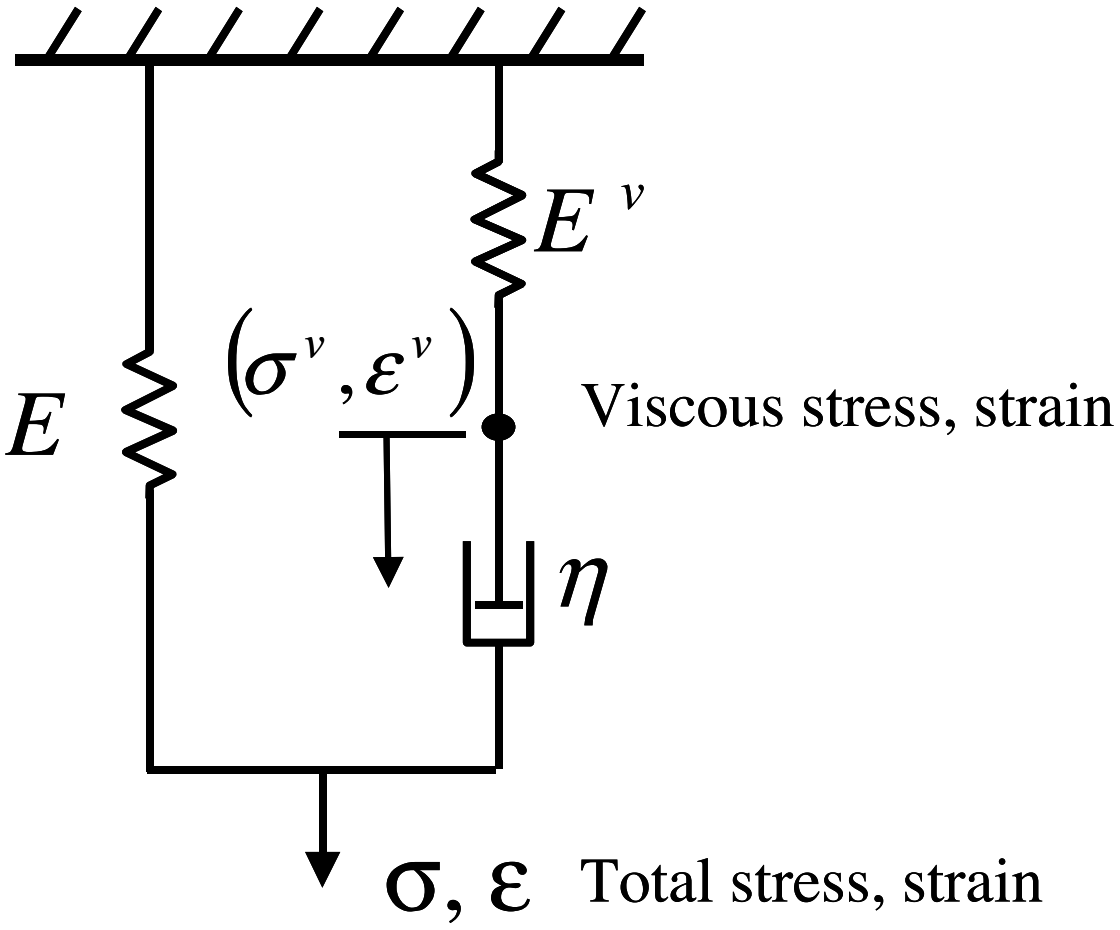

Figure 1. Maxwell solid with one viscous leg.

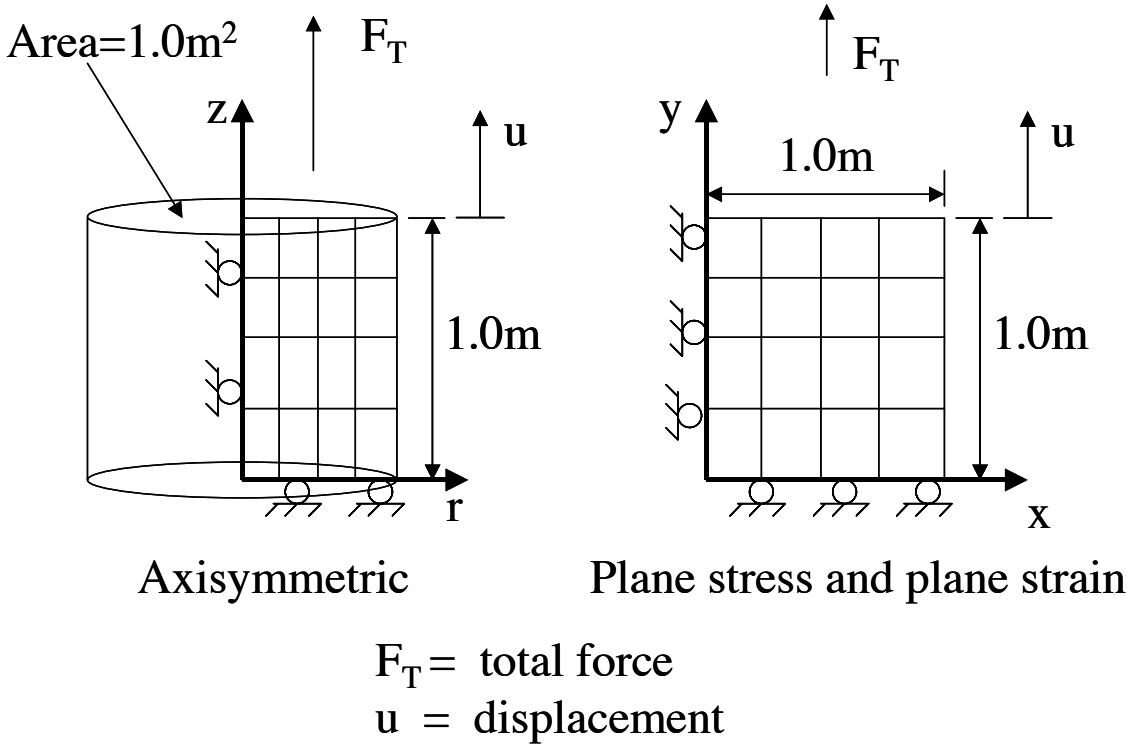

Figure 2. Finite element mesh for uniform axisymmetric, plane stress, and plane strain solids.

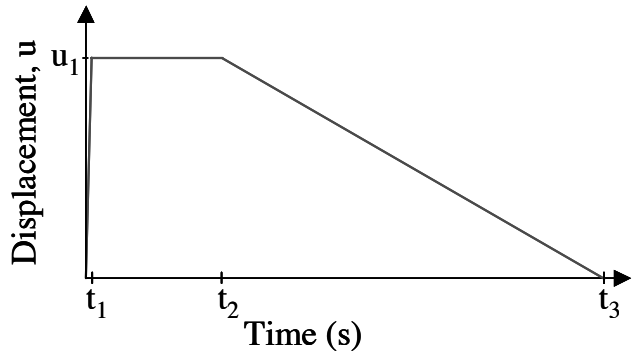

$$t_1 = 0.05\tau$$
$$t_2 - t_1 = 10\tau$$
$$t_3 - t_2 = 30\tau$$

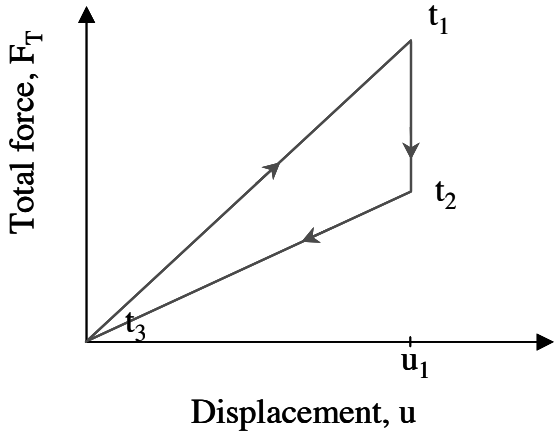

τ = relaxation time constant

Figure 3. Case 1, load displacement loop.

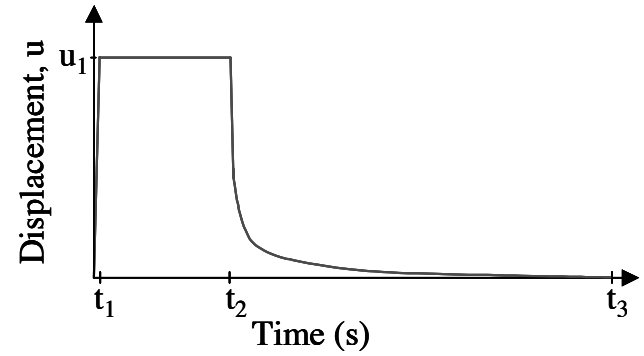

$$t_1 = 0.05\tau$$
$$t_2 - t_1 = 10\tau$$
$$t_3 - t_2 = 0.05\tau$$
$$t_4 - t_3 = 30\tau$$

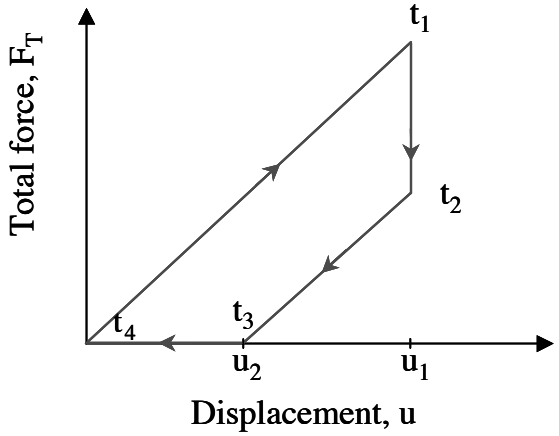

τ = relaxation time constant

Figure 4. Case 2, load displacement loop.

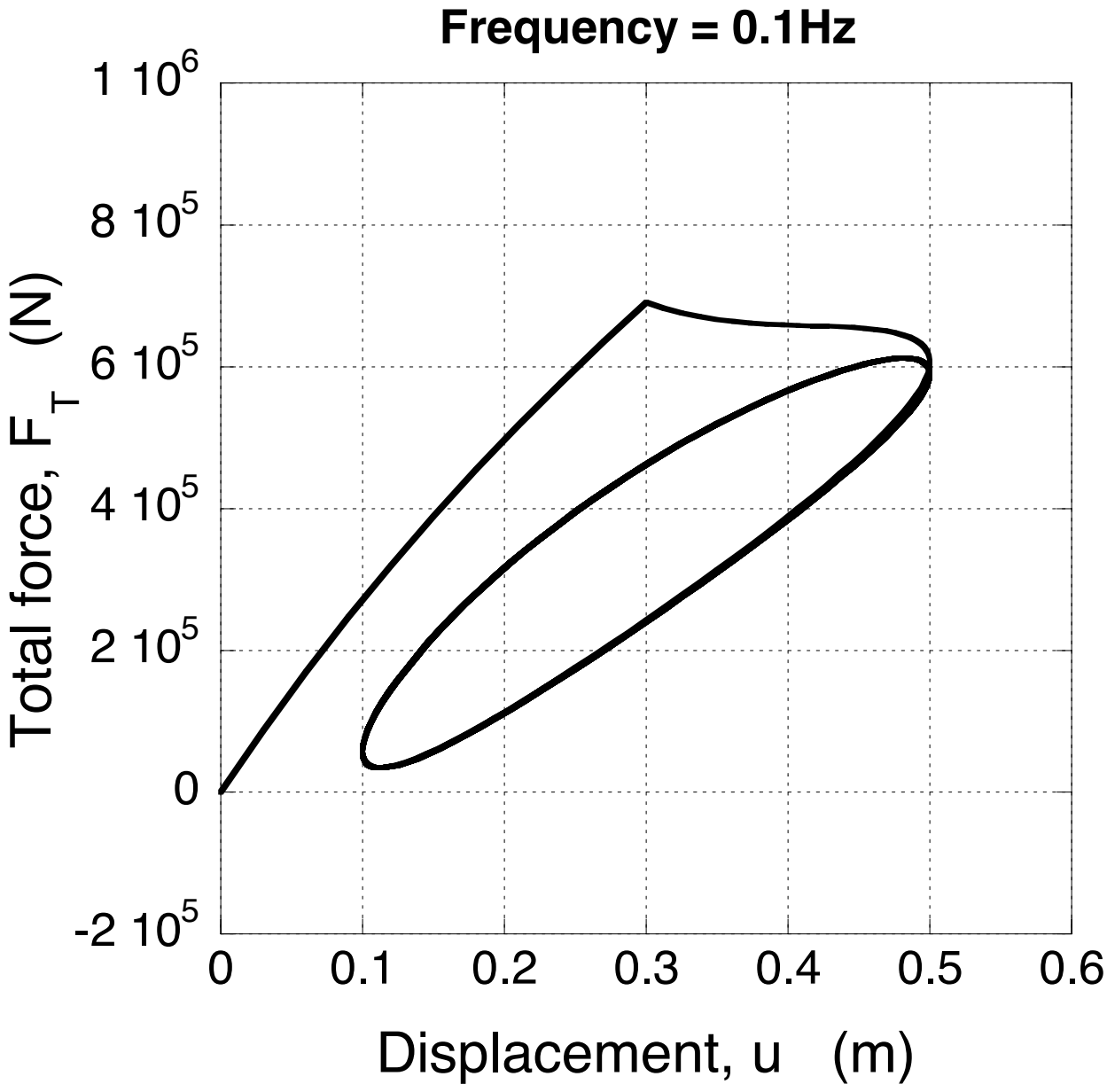

Figure 5. Case 3, load displacement loops, frequency = 0.1 Hz.

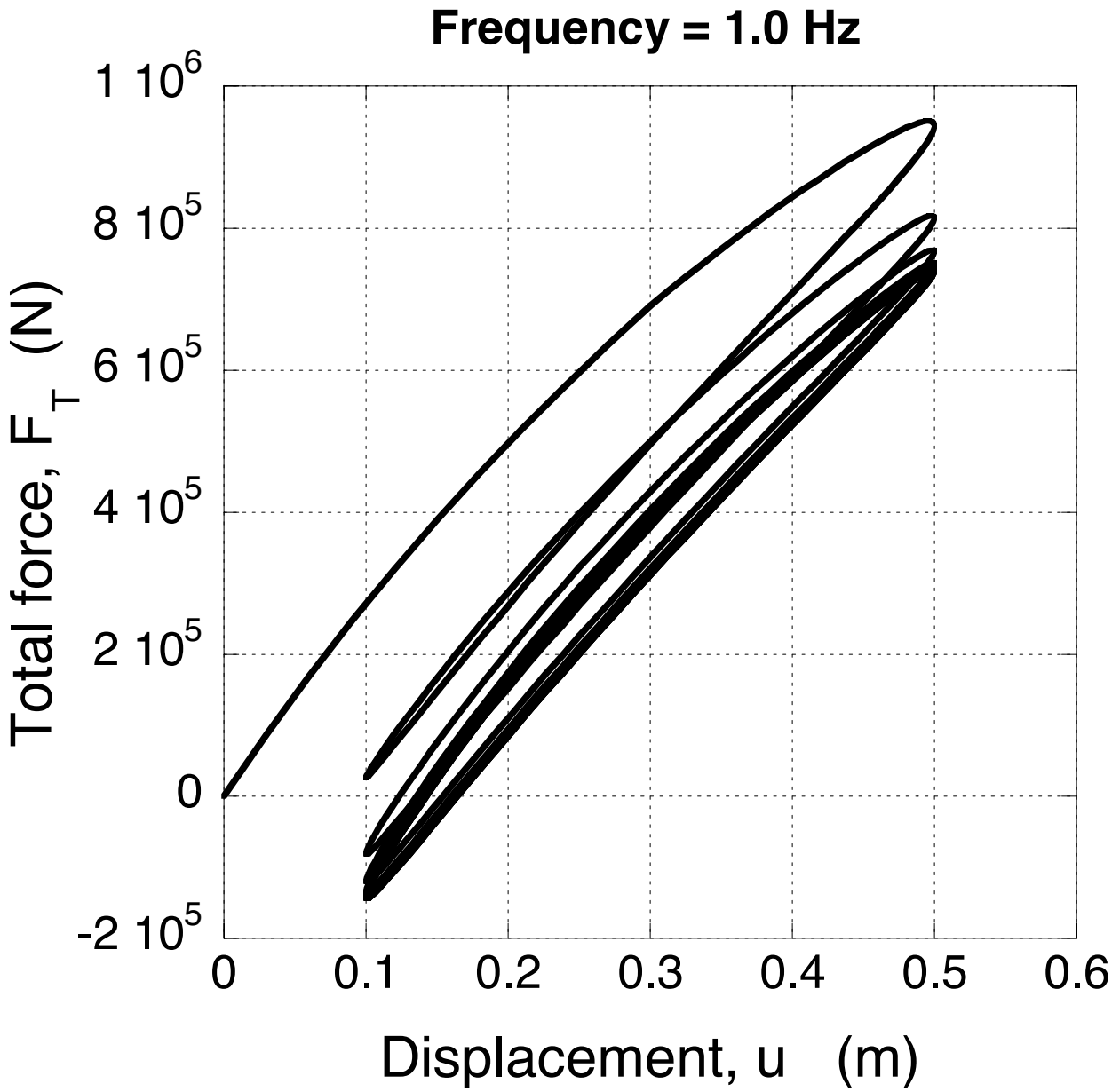

Figure 6. Case 3, load displacement loops, frequency = 1.0 Hz.

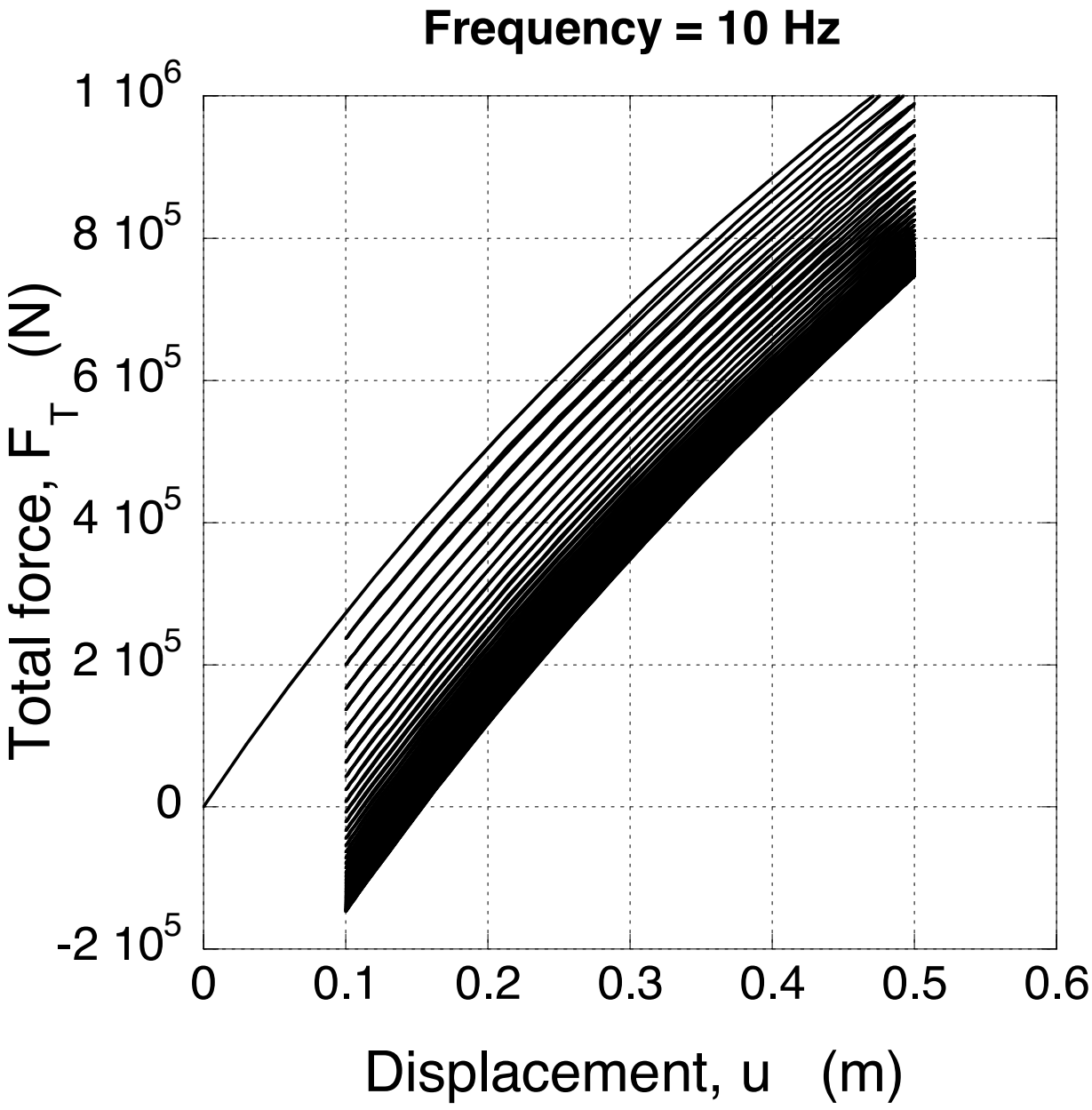

Figure 7. Case 3, load displacement loops, frequency = 10.0 Hz.

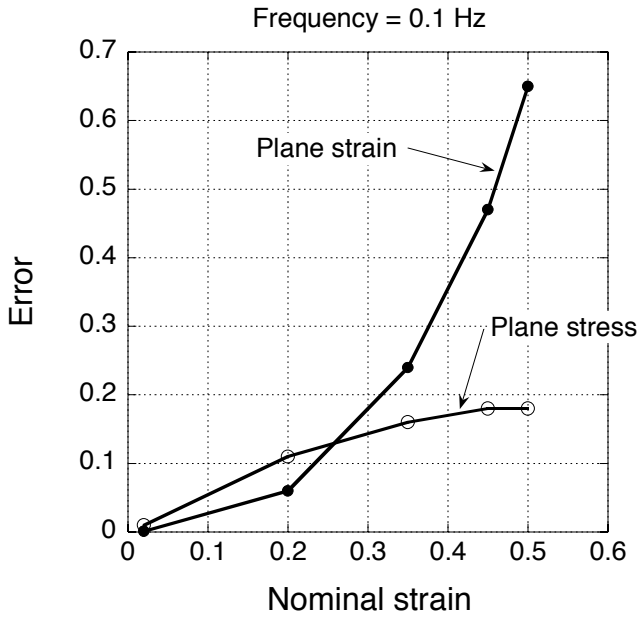

Figure 8. Dissipation error as a function of nominal strain, frequency = 0.1 Hz.

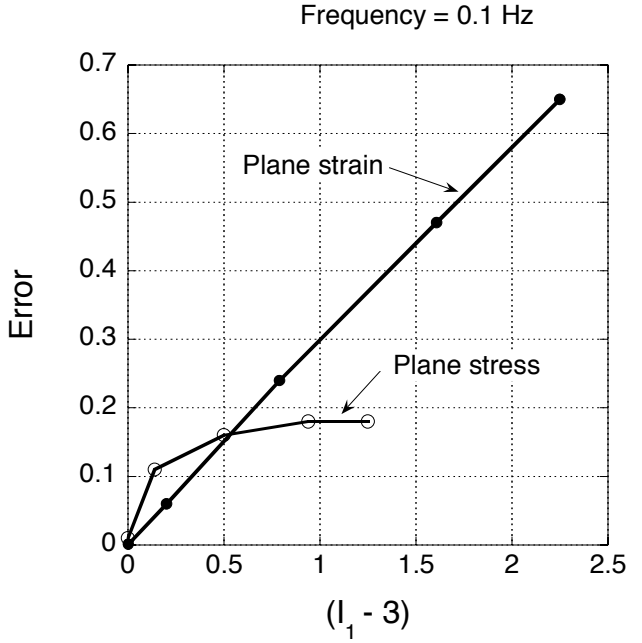

Figure 9. Dissipation error as a function of $(I_1 - 3)$, frequency = 0.1 Hz.

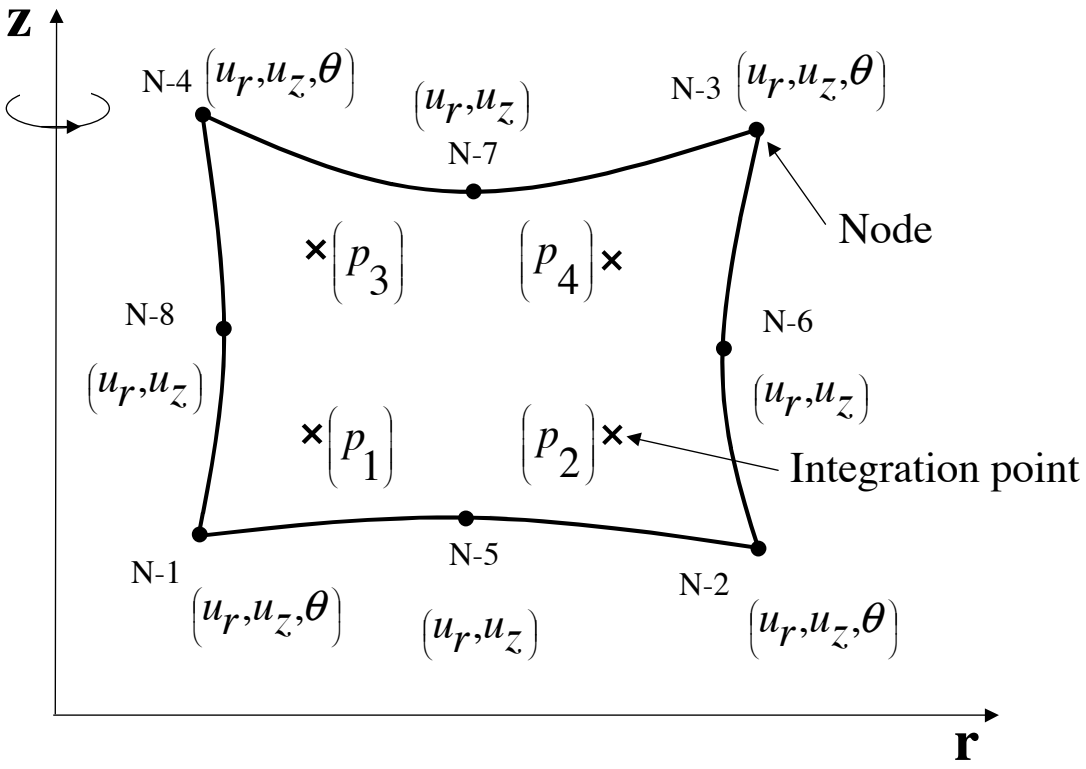

Figure 10. Axisymmetric CAX8RHT element.

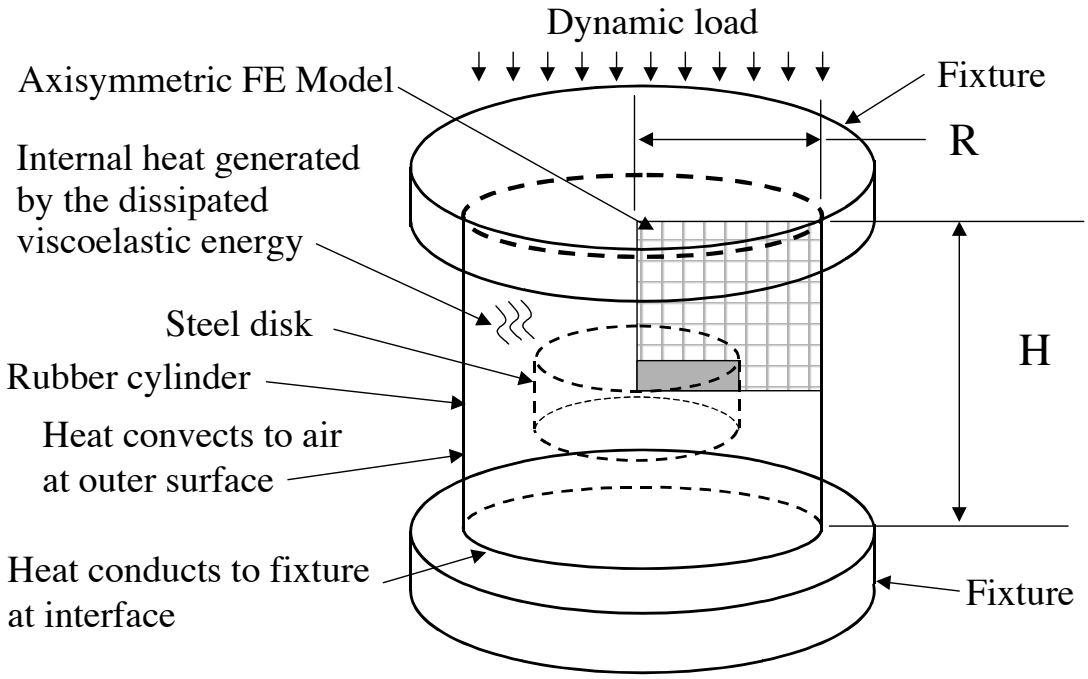

Figure 11. Rubber cylinder, finite element mesh, fixture, and steel disk.

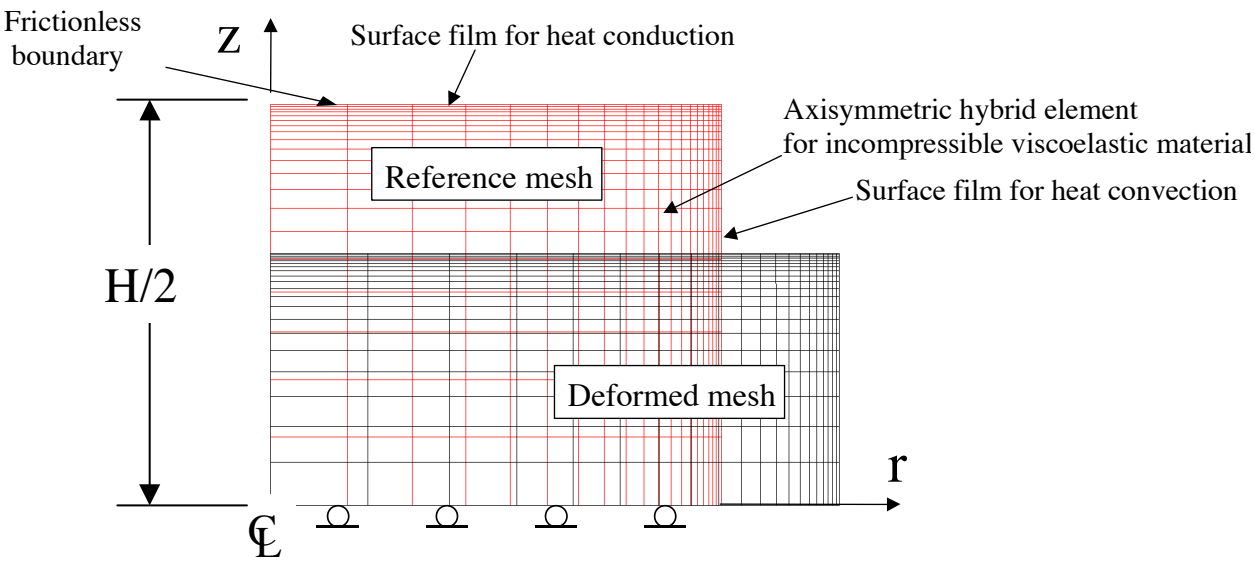

Figure 12. Deformation of a tall uniform cylinder (H = 0.05 m).

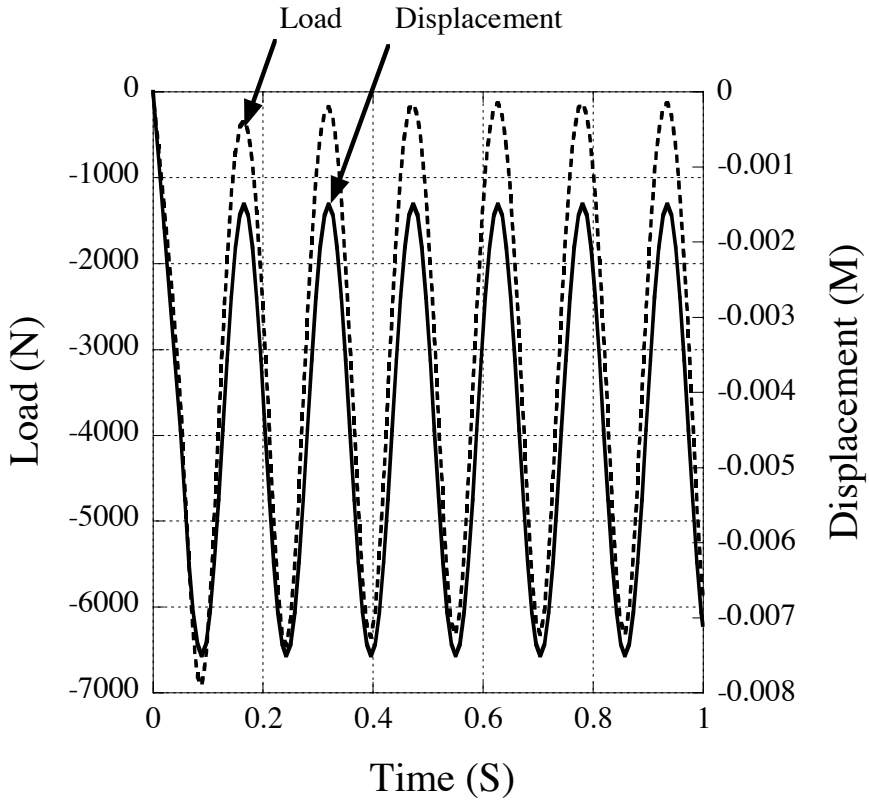

Figure 13. Viscoelastic softening of a tall uniform cylinder (H = 0.05 m).

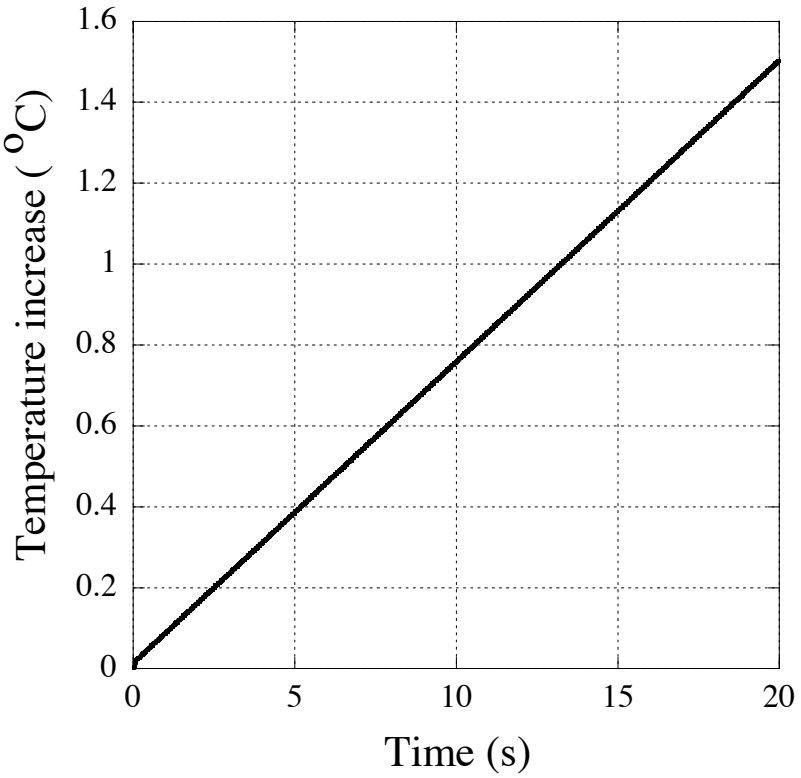

Figure 14. Increase in temperature as a function of time at the center of each uniform cylinder.

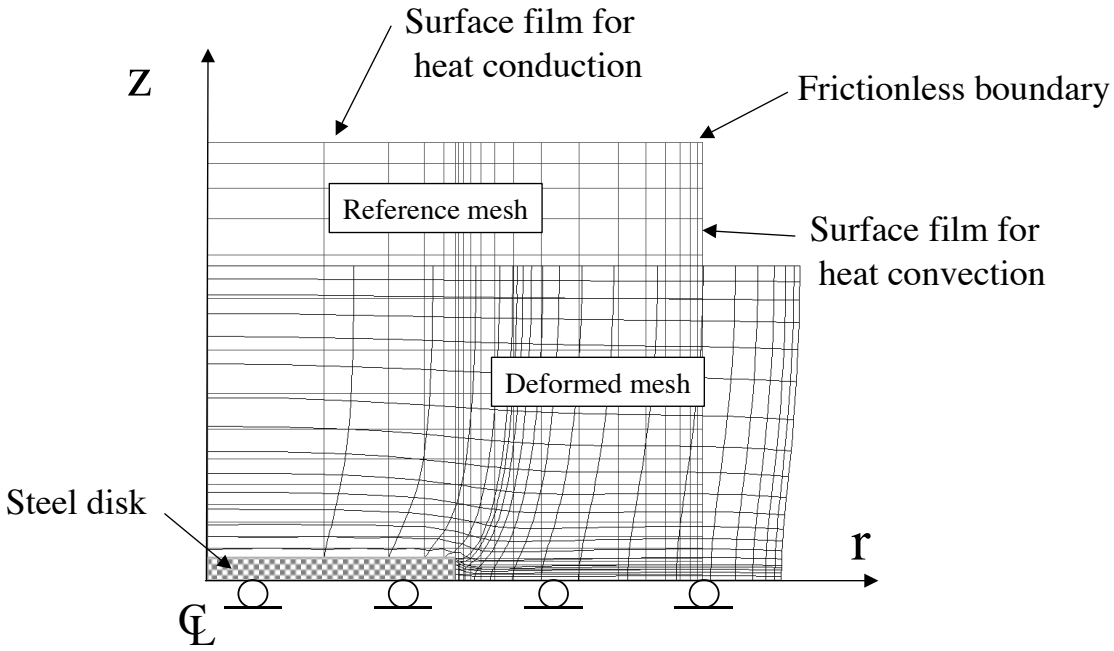

Figure 15. Deformation of a tall cylinder with an internal disk (H = 0.05 m).

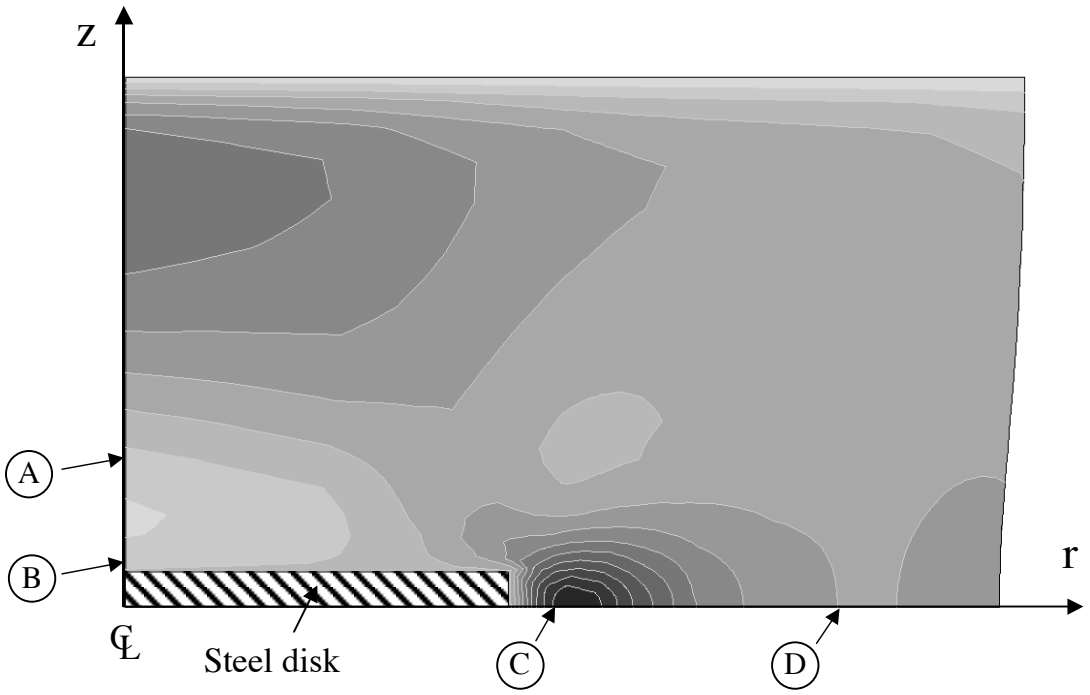

Figure 16. Temperature distribution in a tall cylinder with an internal disk (H = 0.05 m).

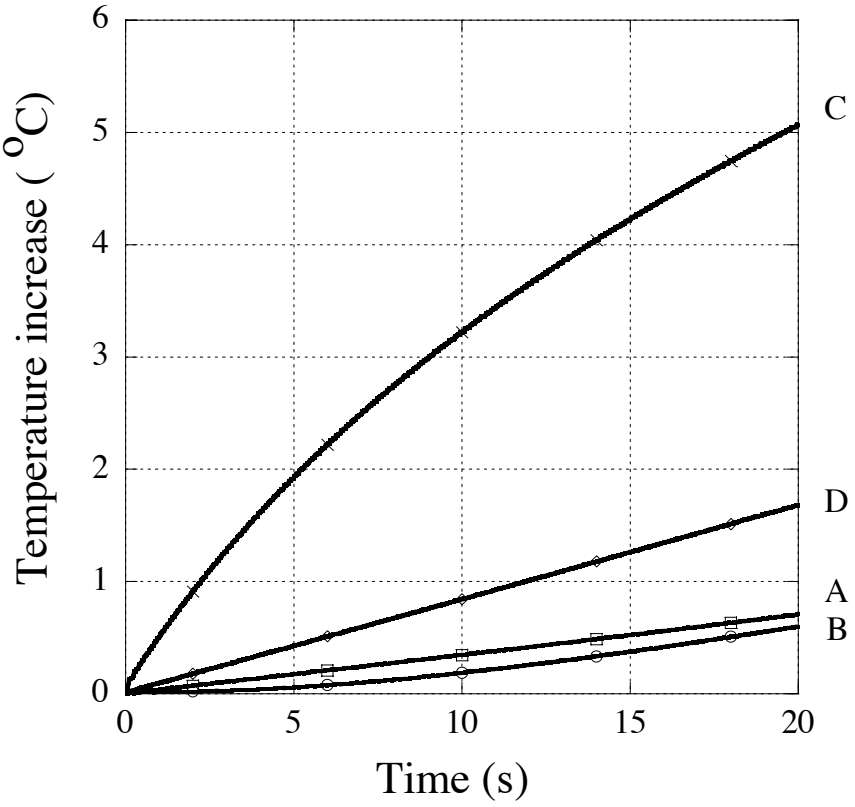

Figure 17. Temperature as a function of time for a tall cylinder with an internal disk (H = 0.05m).

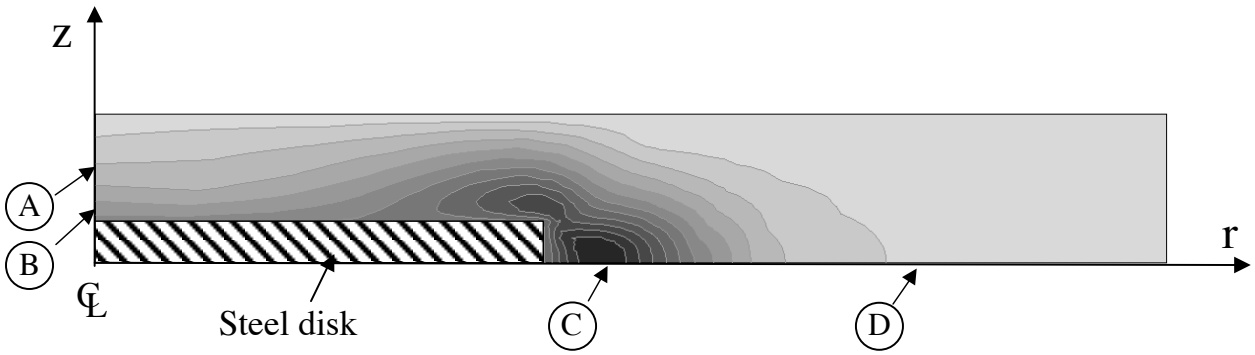

Figure 18. Temperature distribution in a short cylinder with an internal disk (H = 0.0125 m).

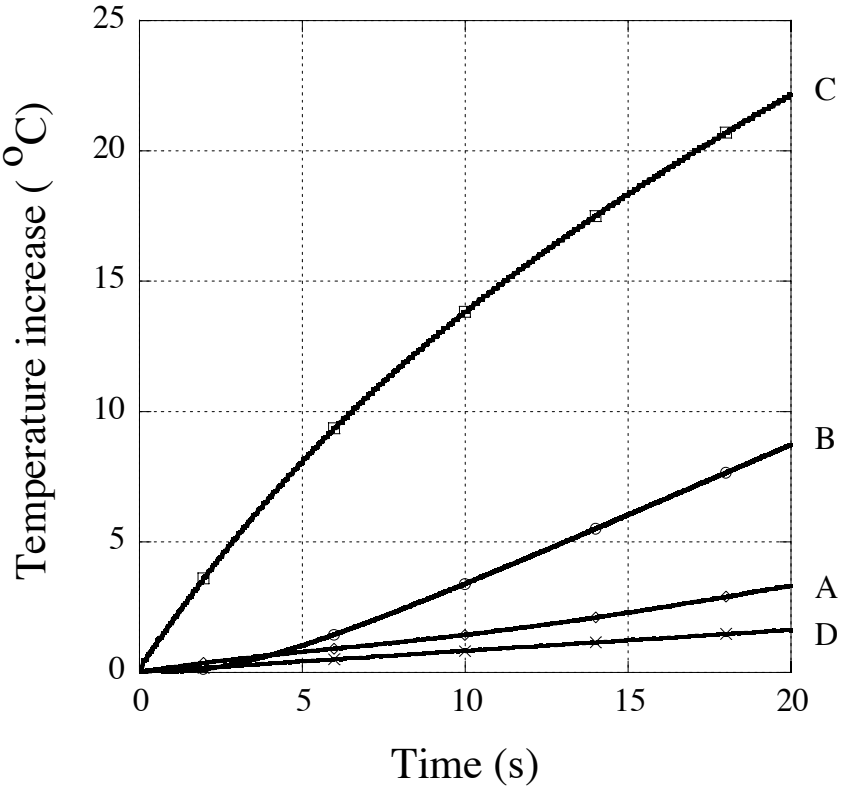

Figure 19. Temperature as a function of time for a short cylinder with an internal disk (H = 0.0125 m).

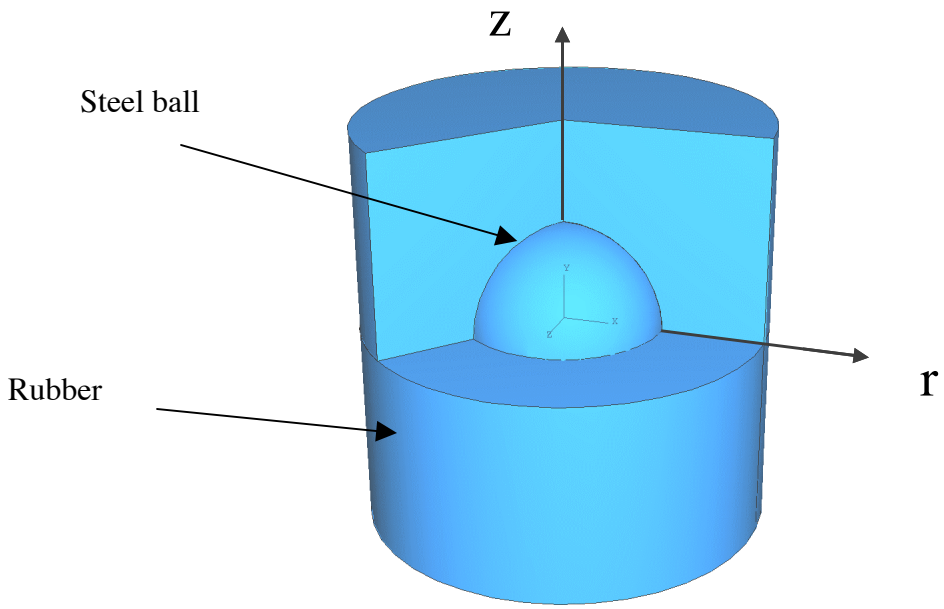

Figure 20. Rubber cylinder with an internal steel ball (H=0.05 m).

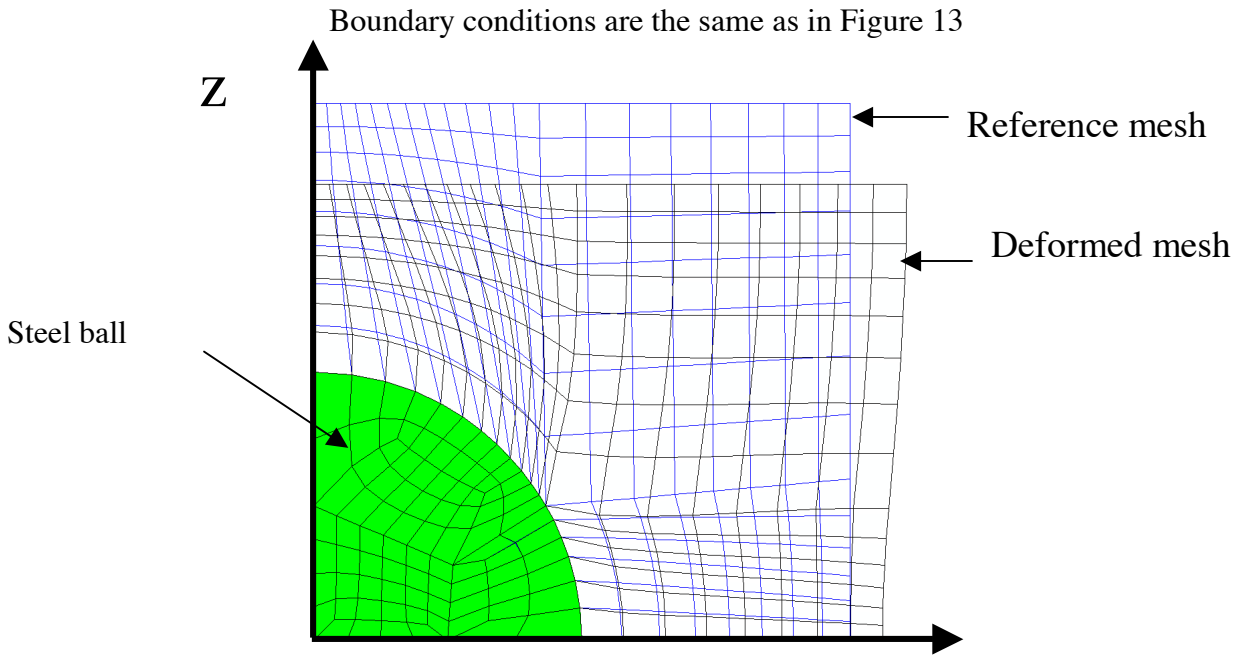

Figure 21. Deformation of a rubber cylinder with an internal steel ball (H=0.05 m).

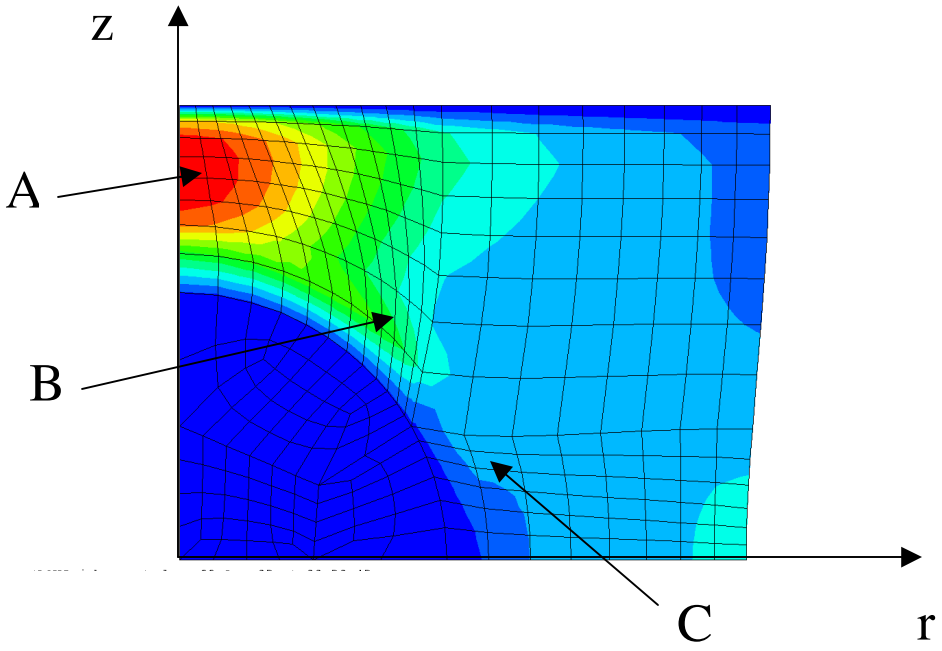

Figure 22. Temperature distribution in a tall rubber cylinder with an internal steel ball (H=0.05 m).

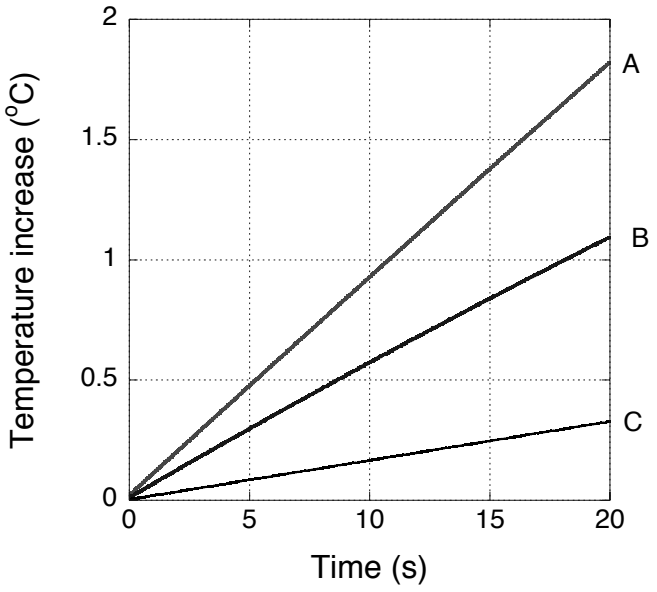

Figure 23. Temperature as a function of time for a tall rubber cylinder with an internal steel ball (H=0.05 m).

REPORT DOCUMENTATION PAGE

Form Approved
OMB No. 0704-0188

1. REPORT DATE *(DD-MM-YYYY)*	2. REPORT TYPE	3. DATES COVERED *(From - To)*
01- 07 - 2003	Technical Memorandum	

4. TITLE AND SUBTITLE

An Approximate Dissipation Function for Large Strain Rubber Thermo-Mechanical Analyses

5a. CONTRACT NUMBER

5b. GRANT NUMBER

5c. PROGRAM ELEMENT NUMBER

6. AUTHOR(S)

Arthur R. Johnson and Tzi-Kang Chen

5d. PROJECT NUMBER

5e. TASK NUMBER

5f. WORK UNIT NUMBER

755-06-00-13

7. PERFORMING ORGANIZATION NAME(S) AND ADDRESS(ES)

NASA Langley Research Center
Hampton, VA 23681-2199

8. PERFORMING ORGANIZATION REPORT NUMBER

L-18308

9. SPONSORING/MONITORING AGENCY NAME(S) AND ADDRESS(ES)

National Aeronautics and Space Administration
Washington, DC 20546-0001

10. SPONSOR/MONITOR'S ACRONYM(S)

NASA

11. SPONSOR/MONITOR'S REPORT NUMBER(S)

NASA/TM-2003-212430 ARL-TR-2998

12. DISTRIBUTION/AVAILABILITY STATEMENT

Unclassified - Unlimited
Subject Category - 39
Availability: NASA CASI (301) 621-0390 Distribution: Standard

13. SUPPLEMENTARY NOTES

An electronic version can be found at http://techreports.larc.nasa.gov/ltrs/ or http:/ntrs.nasa.gov

14. ABSTRACT

Mechanically induced viscoelastic dissipation is difficult to compute. When the constitutive model is defined by history integrals, the formula for dissipation is a double convolution integral. Since double convolution integrals are difficult to approximate, coupled thermo-mechanical analyses of highly viscous rubber-like materials cannot be made with most commercial finite element software. In this study, we present a method to approximate the dissipation for history integral constitutive models that represent Maxwell-like materials without approximating the double convolution integral. The method requires that the total stress can be separated into elastic and viscous components, and that the relaxation form of the constitutive law is defined with a Prony series. Numerical data is provided to demonstrate the limitations of this approximate method for determining dissipation. Rubber cylinders with imbedded steel disks and with an imbedded steel ball are dynamically loaded, and the nonuniform heating within the cylinders is computed.

15. SUBJECT TERMS

Viscoelasticity; Dissipation; Hysteretic heating; Thermo-mechanical heating

16. SECURITY CLASSIFICATION OF:			17. LIMITATION OF ABSTRACT	18. NUMBER OF PAGES	19a. NAME OF RESPONSIBLE PERSON
a. REPORT	b. ABSTRACT	c. THIS PAGE			STI Help Desk (email: help@sti.nasa.gov)
					19b. TELEPHONE NUMBER *(Include area code)*
U	U	U	UU	35	(301) 621-0390